

Line shape and lifetimes of Cr^{3+} luminescence in silicate glasses

M. Yamaga,* B. Henderson, K. P. O'Donnell, and Y. Gao

Department of Physics and Applied Physics, University of Strathclyde, Glasgow G4 0NG, United Kingdom

(Received 9 January 1991; revised manuscript received 19 April 1991)

This paper describes experimental and theoretical studies of the distribution of crystal-field sites occupied by Cr^{3+} ions in silicate glasses. The effects of this site-to-site disorder on the optical band shape of ${}^4T_2 \rightarrow {}^4A_2$ and ${}^2E \rightarrow {}^4A_2$ transitions, luminescence decay time, and their temperature dependences are calculated and compared with experimental results. Since the distribution of the crystal-field splitting, $10Dq$, includes sites having values of the energy separation $E({}^4T_2) - E({}^2E)$, which vary from positive, through zero to negative, it is necessary to take into account the effects of 4T_2 to 2E tunneling induced by spin-orbit coupling and zero-point vibration. Good agreement is obtained between theory and experiment, giving confidence in the assumed distribution of crystal-field sites.

I. INTRODUCTION

Transition-metal ions with the $3d^n$ configuration normally occupy octahedral symmetry sites in insulating crystals. In such sites the multiple-electron energy-level structure is determined by the strength of the octahedral crystal field Dq and the interelectron interaction or Racah parameters, B and C . Solutions to the multiple-electron crystal-field Hamiltonian may be represented on a Tanabe-Sugano diagram in which the normalized multiplet energies $E(\Gamma)/B$, where Γ denotes the irreducible representation of an electronic state, are plotted as a function of Dq/B , for constant value of C/B .¹ Figure 1 is the Tanabe-Sugano diagram for Cr^{3+} ($3d^3$) assuming $C/B = 4.8$; such a diagram may be used to interpret optical absorption and photoluminescence spectra.^{1,2} In general, vibrationally broadened ${}^4A_2 \rightarrow {}^4T_2$ and ${}^4A_2 \rightarrow {}^4T_1$

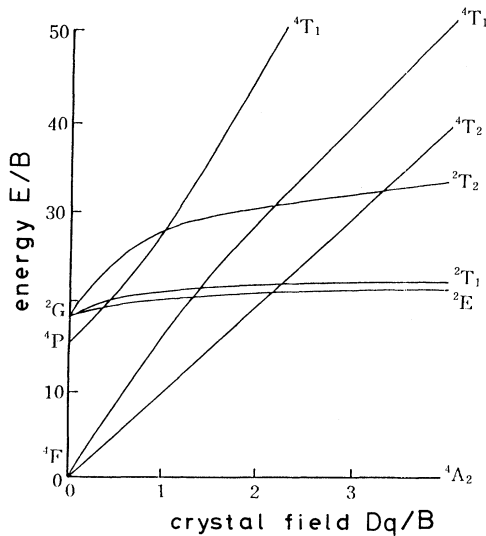


FIG. 1. Energy levels of a $3d^3$ system in an octahedral crystal field.

absorption transitions are observed at wavelengths in the visible region. Much weaker sharp lines are observed, also in the visible region, due to the spin-forbidden absorption transitions ${}^4A_2 \rightarrow {}^2E, {}^2T_1, {}^2T_2$. At low temperatures rapid nonradiative relaxation among the excited states reached in absorption leads to photoluminescence associated with the lowest excited state only. Thus for $Dq/B \ll 2.3$, broadband photoluminescence due to vibronic ${}^4T_2 \rightarrow {}^4A_2$ transitions are observed. Typical of this weak-field situation is the broadband luminescence of Cr^{3+} in $\text{La}_3\text{Lu}_2\text{Ga}_3\text{O}_{12}$ (LLGG) for which the luminescence lifetime is $150 \mu\text{s}$ at 4 K.³ For $Dq/B \gg 2.3$ the spectrum takes the form of narrow zero-phonon lines (R lines) due to ${}^2E \rightarrow {}^4A_2$ transitions and their vibrationally induced sidebands. The lifetime of the R line of Cr^{3+} ions at strong field sites in $\text{Y}_3\text{Al}_5\text{O}_{12}$ (YAG) is 8 ms at 4 K.⁴ For intermediate values of the octahedral crystal field, $Dq/B \approx 2.3$, a mixture of ${}^2E \rightarrow {}^4A_2$ and ${}^4T_2 \rightarrow {}^4A_2$ transitions are observed with lifetime intermediate between those of the pure ${}^4T_2 \rightarrow {}^4A_2$ vibronic transition and ${}^2E \rightarrow {}^4A_2$ R -line transition.^{3,5-9}

The near degeneracy of the excited states ${}^2E, {}^4T_2$ for the values of Dq/B close to 2.3 (see in Fig. 1) has interesting consequences for the emission line shape, intensity of the emission from the 2E level relative to 4T_2 , luminescence decay time, and the temperature dependence of these properties. For example, the energy separation $E({}^4T_2) - E({}^2E)$ of $\text{Cr}^{3+}:\text{Gd}_3\text{Sc}_2\text{Ga}_3\text{O}_{12}$ (GSGG) was estimated to be $70-100 \text{ cm}^{-1}$.^{3,6-8} In this case the observed photoluminescence spectrum is a superposition of a broad ${}^4T_2 \rightarrow {}^4A_2$ band on the ${}^2E \rightarrow {}^4A_2$ R line and its vibronic sideband even at 1.6 K where the thermal energy is relatively small compared to the energy separation. The ratio of the total intensity of the broadband relative to that of the R line and its vibronic sideband is constant below 30 K. In addition, the lifetime of the broadband at low temperature ($230 \mu\text{s}$) is equal to that of the R line and is intermediate between those of YAG and LLGG. The authors explained these experimental results in terms of a tunneling model.⁶⁻⁸ The essential characteristics of this model are as follows. The 2E and 4T_2 excited states of

Cr^{3+} ions, when represented by Born-Oppenheimer (BO) vibronic wave functions, are separated by a potential barrier. For intermediate crystal field, these levels are close together in energy and the barrier is lowered. When the barrier height is comparable to the average phonon energy, tunneling occurs easily between the two states through the zero-point vibration and spin-orbit coupling. Thus, the mixing of the BO vibronic wave functions influences the line shapes, and lifetimes of the emission from the lowest excited state of Cr^{3+} ions. Since the mixing coefficients are temperature dependent, then so too are line shapes, luminescence intensities, and luminescence decay time.

In two recent papers^{10,11} the authors have discussed the optical properties of Cr^{3+} ions in approximately octahedral sites in a variety of inorganic glasses. Both absorption and emission spectra are inhomogeneously broadened as a consequence of multisite occupancy by Cr^{3+} ions. A further consequence of this disorder is that luminescence decay is nonexponential. The luminescence results for Cr^{3+} -doped borate, fluoride, phosphate, and silicate glasses were interpreted in terms of Cr^{3+} ions occupying sites in which the mean crystal field Dq/B may be ≤ 2.3 . This had the inevitable consequence that some Cr^{3+} ions occupied sites in which the 2E and 4T_2 states were close to degeneracy. Although the theoretical analysis for intermediate crystal field $Dq/B \approx 2.3$ was developed for Cr^{3+} emitters in single-crystal garnets,⁶⁻⁸ it necessarily applies also to Cr^{3+} -doped glasses. The earlier papers^{10,11} discussed crystal-field effects apparent in absorption and emission spectra of Cr^{3+} ions in differential glasses and measurements of the temperature dependence of the homogeneous width of R line. This latter feature reflects the coupling of the electronic levels to low-energy, two-level vibration systems which occur with high density in many inorganic glasses. The present paper, an extension of the earlier work, is concerned with how the distribution of crystal-field sites occupied by Cr^{3+} ions affects the band shape and decay characteristics.

II. THEORY

A. Line shape of broadband absorption and emission

The difference in electron-phonon coupling between ground 4A_2 and excited 4T_2 states of Cr^{3+} ions leads to

$$I_{ab}(E) = \frac{I_{ab}^0}{\sqrt{2\pi}\Gamma} \int_0^\infty P(10Dq) \exp\left[-\frac{(E-10Dq)^2}{2\Gamma^2}\right] d(10Dq) \quad (4)$$

$$= \frac{I_{ab}^0}{\sqrt{2\pi}\Gamma} \int_0^\infty P'(10Dq, E) \exp\left[-\frac{[E-(10Dq)_0]^2}{2(\Gamma^2+\gamma^2)}\right] d(10Dq), \quad (5)$$

where

$$P'(10Dq, E) = \frac{1}{\sqrt{2\pi}\gamma} \exp\left[-\frac{\Gamma^2+\gamma^2}{2\Gamma^2\gamma^2} \left[10Dq - \frac{\Gamma^2(10Dq)_0 + \gamma^2 E}{\Gamma^2+\gamma^2}\right]^2\right]. \quad (6)$$

broadband optical transitions between these states. At $T=0$ K the line shape functions of absorption and emission bands² are

$$I_{\pm}(E) = I_{\pm}^0 \sum_m \frac{\exp(-S)S^m}{m!} \delta(E_0 \pm m\hbar\omega - E), \quad (1)$$

where $+$ or $-$ refer to absorption or emission bands, $E_0 = 10Dq - S\hbar\omega$, $10Dq$ is the crystal-field splitting, S is the Huang-Rhys parameter, and $\hbar\omega$ is the average phonon energy. Following Sugano, Tanabe, and Kamimura¹ Dq is calculated to be proportional to a^{-5} , where a is the distance between Cr^{3+} and O^{2-} . Assuming strong electron-phonon coupling, i.e., $S \gg 1$ and taking account of the width of each phonon-assisted line, the line-shape functions are approximately represented by

$$I_{\pm}(E) = \frac{I_{\pm}^0}{\sqrt{2\pi}\Gamma} \exp\left[-\frac{(E-\varepsilon_{\pm})^2}{2\Gamma^2}\right], \quad (2)$$

where ε_{\pm} are the energies of the Frank-Condon transitions and full width at half maximum (FWHM) of the Gaussian is $(2\sqrt{2\ln 2})\Gamma$.

Here we consider the change in line-shape function that derives from including the disorder inherent in the distribution of Cr^{3+} ions in glasses. In practice, disorder reflects the distribution of the crystal-field splitting, $10Dq$. The probability that the Cr^{3+} ions occupy sites with splitting $10Dq$ is assumed to be

$$P(10Dq) = \frac{1}{\sqrt{2\pi}\gamma} \exp\left[-\frac{[10Dq - (10Dq)_0]^2}{2\gamma^2}\right], \quad (3)$$

where $(10Dq)_0$ is the energy of the Cr^{3+} sites with maximum probability and γ is the width of the distribution. The vibrational relaxation energy, $S\hbar\omega \approx 2000$ cm^{-1} , is much smaller than the mean crystal-field energy, $(10Dq)_0 \approx 16000$ cm^{-1} . It is assumed that the distribution of the relaxation energy, $S\hbar\omega$, of Cr^{3+} sites created by disorder is negligibly small. The absorption line-shape function with $\varepsilon_+ = 10Dq$ in Eq. (2), including the effect of disorder represented by Eq. (3), becomes

The modified absorption band shape is a Gaussian with peak energy $(10Dq)_0$ and width $\Gamma_{ab} = \sqrt{\Gamma^2 + \gamma^2}$. This is formally equivalent to the convolution of a Gaussian with a Gaussian, necessarily giving the same result.

The distribution of Cr³⁺ sites excited by laser beam with excitation energy E_{ex} , given by $P'(10Dq, E_{ex})$, has a maximum value at

$$10Dq = [\Gamma^2(10Dq)_0 + \gamma^2 E_{ex}] / (\Gamma^2 + \gamma^2) .$$

Assuming that the excited electron relaxes immediately to the lowest vibronic level of the excited electronic state and that the distribution of the Cr³⁺ sites does not change in this process gives the photon energy at the emission band peak as

$$\varepsilon_- = \frac{\Gamma^2(10Dq)_0 + \gamma^2 E_{ex}}{\Gamma^2 + \gamma^2} - (2S - 1)\hbar\omega , \quad (7)$$

where $(2S - 1)\hbar\omega$ is the Stokes shift energy.² The emission bandwidth, Γ_{em} , is,

$$\Gamma_{em} = \sqrt{\Gamma^2 + \gamma^2} , \quad (8)$$

where

$$\frac{1}{\gamma'^2} = \frac{1}{\gamma^2} + \frac{1}{\Gamma^2} . \quad (9)$$

B. Radiative and nonradiative decays of Cr³⁺ sites

As the barrier separating the two excited states 4T_2 and 2E is lowered until it becomes comparable with the phonon energy, the BO adiabatic approximation becomes invalid. Tunneling occurs between the two potential minima through zero-point vibration and spin-orbit coupling and mixes the BO vibronic wave functions.⁶⁻⁸ The admixed wave functions of Cr³⁺ ions at sites with crystal-field splitting $10Dq = E_i$ are given by

$$\Psi_1^i(r_i, R_i) = \alpha_i \Psi_E^i(r_i, R_i) + \beta_i \Psi_T^i(r_i, R_i) , \quad (10)$$

$$\Psi_2^i(r_i, R_i) = \beta_i \Psi_E^i(r_i, R_i) - \alpha_i \Psi_T^i(r_i, R_i) , \quad (11)$$

$$\alpha_i = \frac{\Delta_i + (\Delta_i^2 + 4\delta^2)^{1/2}}{\{[\Delta_i + (\Delta_i^2 + 4\delta^2)^{1/2}]^2 + 4\delta^2\}^{1/2}} , \quad (12)$$

$$\beta_i = \frac{-2\delta}{\{[\Delta_i + (\Delta_i^2 + 4\delta^2)^{1/2}]^2 + 4\delta^2\}^{1/2}} , \quad (13)$$

with

$$\Delta_i = E_i({}^4T_2) - E_i({}^2E) = [E_i - (S - \frac{1}{2})\hbar\omega] - E_i({}^2E) . \quad (14)$$

In these equations $\Psi_E^i(r_i, R_i)$, $\Psi_T^i(r_i, R_i)$, $E_i({}^2E)$, and $E_i({}^4T_2)$ are the pure vibronic wave functions and energy levels of the 2E and 4T_2 states at Cr³⁺ sites with $10Dq = E_i$ in the absence of tunneling, and α_i and β_i are mixing coefficients determined by the energy separation Δ_i and the tunneling splitting, 2δ . The transition probabilities^{7,8} from $\Psi_1^i(r_i, R_i)$ and $\Psi_2^i(r_i, R_i)$ in Eqs. (10) and

(11) are given by

$$\frac{1}{\tau_1^i} = \frac{\alpha_i^2}{\tau_E^i} + \frac{\beta_i^2}{\tau_T^i} \quad (15)$$

and

$$\frac{1}{\tau_2^i} = \frac{\beta_i^2}{\tau_E^i} + \frac{\alpha_i^2}{\tau_T^i} , \quad (16)$$

where τ_E^i and τ_T^i are the lifetime of the pure vibronic states of the Cr³⁺ site with $10Dq = E_i$ in the absence of tunneling. The total intensities of the R line and its vibronic sideband and the broadband of the Cr³⁺ site following pulse excitation as functions of temperature T and time t are given by⁸.

$$I_E^i = \frac{n_0^i}{\tau_E^i} \frac{\alpha_i^2 + \beta_i^2 \exp(-\Delta E_i/kT)}{1 + \exp(-\Delta E_i/kT)} \exp\left[-\frac{t}{\tau_i}\right] , \quad (17)$$

$$I_T^i = \frac{n_0^i}{\tau_T^i} \frac{\beta_i^2 + \alpha_i^2 \exp(-\Delta E_i/kT)}{1 + \exp(-\Delta E_i/kT)} \exp\left[-\frac{t}{\tau_i}\right] , \quad (18)$$

$$\frac{1}{\tau_i} = \frac{1/\tau_1^i + (1/\tau_2^i) \exp(-\Delta E_i/kT)}{1 + \exp(-\Delta E_i/kT)} + W_{nr}^i(T) , \quad (19)$$

where n_0^i is the population number of excited Cr³⁺ site under steady-state conditions, ΔE_i is energy separation between 2E and 4T_2 states of the Cr³⁺ site with $10Dq = E_i$ including tunneling effect, and $W_{nr}^i(T)$ is the nonradiative transition rate.^{12,13} The population number n_0^i is the product of the pumping rate R_i , the luminescence lifetime τ_i , and the ground-state population, N_{gr} , at the Cr³⁺ site; i.e.,

$$n_0^i = R_i N_{gr}^i \tau_i , \quad (20)$$

where

$$N_{gr}^i = N P_i . \quad (21)$$

N is the concentration of Cr³⁺ ions in the glass and P_i is the probability of occupation of sites for which $10Dq = E_i$ in Eq. (3). The pumping rate R_i produced by a laser beam with energy E_{ex} is proportional to $P'(E_i, E_{ex})$ in Eq. (6). Then the decay of R line and broadband including the effect of disorder is given by

$$I_E(t, T) = \int_0^\infty I_E^i dE_i , \quad (22)$$

$$I_T(t, T) = \int_0^\infty I_T^i dE_i . \quad (23)$$

In general, the nonradiative transition rate, $W_{nr}^i(T)$,^{12,13} is represented by

$$W_{nr}^i(T) = R^2 \exp[-S(1+2m)] \left[\frac{1+m}{m} \right]^{p/2} \times I_p[2S\sqrt{m(m+1)}] , \quad (24)$$

$$m = \frac{1}{\exp(\hbar\omega/kT) - 1} , \quad (25)$$

$$p = \frac{E_i - S\hbar\omega}{\hbar\omega} , \quad (26)$$

where the disorder is assumed to influence only the values of $10Dq$, the values of S and R being assumed constant.

III. EXPERIMENTAL PROCEDURES

Silicate glasses have wide ranges of composition in which modifiers such as Li_2O , Na_2O , or K_2O , are added to break up the random network of SiO_2 tetrahedra, and stabilizers such as Al_2O_3 or B_2O_3 prevent crystallization. Si-O-Si bonds are also broken by CaO and replaced by $\text{Si-O}^- \text{-Ca}^{++} \text{-O}^- \text{-Si}$. Network modifiers are especially important in Cr^{3+} -doped glasses since in breaking up the SiO_2 network they enable the $3d^3$ ion to occupy "octahedrally" coordinated sites.^{14,15} The compositions (in mol.%) of the silicate glass used in this study are SiO_2 (68.59), Li_2O (15.74), CaO (10.73), Al_2O_3 (4.91), and Cr_2O_3 (0.03). The glass sample was provided by Dr. S. E. Stokowski at Lawrence Livermore Laboratory.

The general optical absorption and photoluminescence features of this and other glasses have been discussed in detail by the authors.^{10,11} Optical absorption measurements were carried out on 1-mm-thick polished-glass samples at 300 K using a commercial dual beam spectrophotometer operating in the wavelength range 185–1000 nm. Photoluminescence measurements were carried out on glass samples cut and polished to dimensions of $1 \times 2 \times 5 \text{ mm}^3$. For single-line excitation it was possible to select any of the resonance lines from the Ar^+ -ion laser. Other wavelengths were obtained from the dye laser which used rhodamine 6G dye as the laser gain medium. Neutral density filters were used to keep the excitation density to a low value so as to minimize sample heating by the laser beam and to avoid nonlinear transient bleaching effects. The photoluminescence was detected in the right-angle geometry configuration so as to minimize specular reflection at the excitation wavelength and any stray plasma radiation from the Ar^+ -ion laser. The laser excitation beam was mechanically chopped at frequencies ranging from 100 to 3 kHz. The luminescence from the glass samples was focused onto the entry slit of a 1-m scanning monochromator and detected at the exit slit using a GaAs photomultiplier tube and a current amplifier. The signal after amplification was processed using a phase-sensitive detector or boxcar averager. Such facilities enabled the wavelength distribution of the luminescence signal to be measured and its decay pattern recorded following pulsed excitation. The photoluminescence measurements were made at 13 K from samples enclosed in the vacuum space of a cryorefrigerator capable of working at temperatures in the range 13–300 K. Control of temperature was within $\pm 1 \text{ K}$.

IV. RESULTS AND DISCUSSION

A. Absorption and emission spectra

Figure 2 compares typical optical absorption and emission spectra of Cr^{3+} ions excited at 300 K with the 488-nm Ar^+ line in a silicate glass (a), and in $\text{Gd}_3\text{Sc}_2\text{Al}_3\text{O}_{12}$ (GSAG) (b). These results are similar to spectra in the published literature (see, for example, Andrews, Lem-

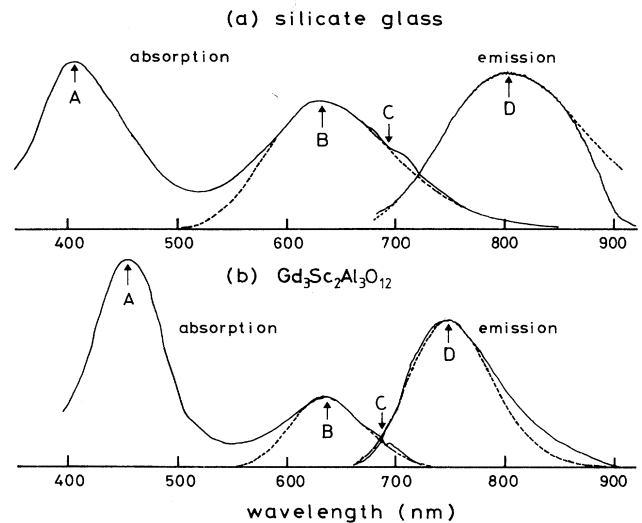


FIG. 2. Absorption and emission spectra of Cr^{3+} at 300 K in (a) silicate glass in comparison with those in (b) $\text{Gd}_3\text{Sc}_2\text{Al}_3\text{O}_{12}$ (GSAG) crystal. The dotted curves calculated using Gaussians are fitted to the observed spectra.

picki, and McCollum¹⁶). Two absorption bands denoted by A and B in Fig. 2 are due to transitions from the 4A_2 ground state to the 4T_1 and 4T_2 excited states of Cr^{3+} ions, respectively. Also evident are R -line absorptions denoted by C, which at 300 K are much weaker and broader than at low temperature. The dotted curves are calculated to fit the observed absorption and emission bands using the parameters $\Gamma_{ab} = 1400 \text{ cm}^{-1}$, $\Gamma_{em} = 1000 \text{ cm}^{-1}$, and $\Gamma_{ab} = 800 \text{ cm}^{-1}$, $\Gamma_{em} = 680 \text{ cm}^{-1}$ for the Cr^{3+} :silicate glass and for the Cr^{3+} :GSAG crystal, respectively. At 300 K the fluorescence spectra in Fig. 2 are almost entirely due to the broadband $^4T_2 \rightarrow ^4A_2$ transition. The difference between the observed and calculated emission band shapes for the Cr^{3+} :silicate glass above 860 nm is due to the rapid decrease in sensitivity of the photomultiplier in this wavelength range ($\lambda > 860 \text{ nm}$). The deviation of the calculated curve from the observed emission band in the Cr^{3+} :GSAG crystal occurs in the longer-wavelength range. This suggests that the observed spectrum fits the curve calculated using Eq. (1) with $S \sim 5$. The widths of absorption and emission bands of Cr^{3+} in the silicate glass are rather larger than those in the GSAG crystal, because of both to the large Stokes shift compared with the GSAG crystal and the disorder of the octahedral environment of Cr^{3+} sites in the glass. The large Stokes shift is important for nonradiative decay, as is discussed in a following section.

Figure 3 shows the emission spectra of the Cr^{3+} :silicate glass measured at 13 K using different excitation wavelengths. At this temperature there is evidence of weak R -line emission denoted by A in Fig. 3 as well as very strong emission in the $^4T_2 \rightarrow ^4A_2$ band denoted by

TABLE I. Parameters of the emission broadband of Cr^{3+} ions in the silicate glass.

Excitation energy, E_{ex} (cm^{-1})	15 650	16 080	17 270
Observed			
Width, Γ_{em} (cm^{-1})	1000	1000	1000
Peak energy, ϵ_{-} (cm^{-1})	12 350	12 370	12 470
Calculated			
Width, Γ (cm^{-1})	965	965	965
Width, γ' (cm^{-1})	270	270	270
Peak energy, ϵ_{-} (cm^{-1})	12 350	12 370	12 470

B. The relative intensities of *R* line and broadband depend on excitation wavelength, *R*-line emission being more pronounced at 579 and 622 nm than at 488 and 639 nm. The ${}^4T_2 \rightarrow {}^4A_2$ peak also shifts with excitation wavelength.^{10,11} The dotted curves are the calculated Gaussian band shapes. As noted above, the deviation between calculated and observed curves at longer wavelength is due to the decreased photomultiplier sensitivity. The fitted parameters (the peak energy ϵ_{-} and the width, Γ_{em} , of the emission band) are summarized in Table I. The relation between the excitation energy E_{ex} and the peak en-

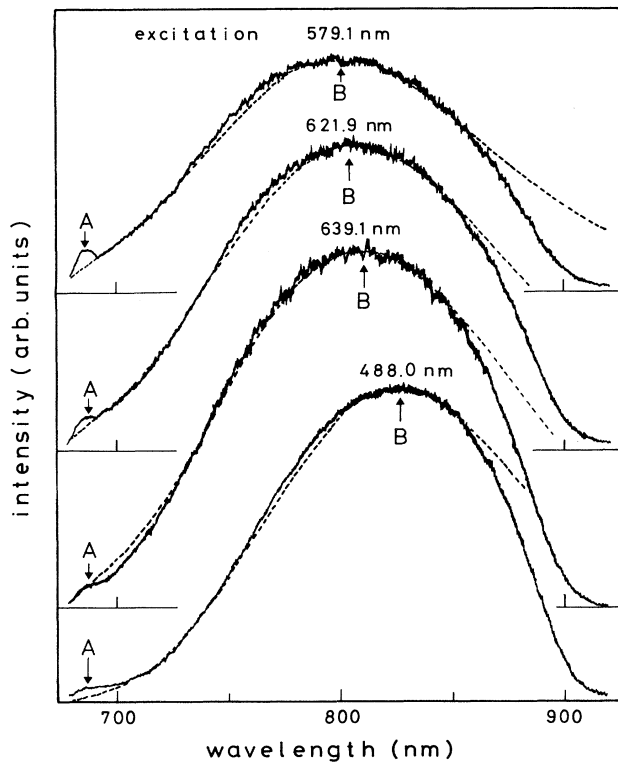


FIG. 3. Emission spectra of Cr^{3+} :silicate glass at 13 K excited at different wavelengths. The dotted curves are the calculated Gaussians. The fitting parameters are summarized in Table I.

ergy ϵ_{-} , of the emission is given by Eq. (7). The value of $(10Dq)_0$ is equal to the photon energy at the peak of the absorption band where the magnitude of the Stokes shift, ${}^2(2S-1)\hbar\omega$, is the energy separation between peaks of absorption and emission bands. The estimated values of intrinsic width Γ of emission band and width γ' of disorder distribution are also summarized in Table I.

Figure 4(a) shows the temperature dependence of the emission spectra of the Cr^{3+} :silicate glass excited at 488 nm. The total intensity of the emission band decreases gradually with increasing temperature. The intensity at 300 K is reduced to about 25% of the intensity observed at 13 K and the wavelength at the peak of the emission band is shifted to shorter wavelength. The wavelength at the peak of the broadband is expected to be shifted to longer wavelength as a consequence of lattice expansion with increasing temperature.^{5,9} These results are explained as due to the excited Cr^{3+} sites with lower emission energy ϵ_{-} relaxing nonradiatively to the ground state. We assume that the distribution of the excited

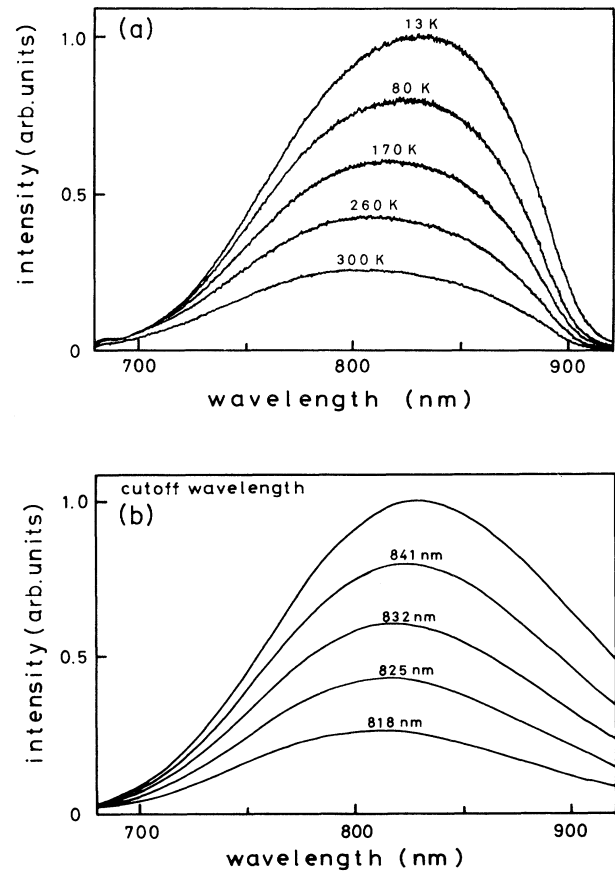


FIG. 4. (a) Emission spectra of Cr^{3+} :silicate glass excited at 488 nm at different temperatures. (b) Emission line shapes are calculated using Eq. (27), $\epsilon_{-}=12\,050\text{ cm}^{-1}$, $\gamma'=230\text{ cm}^{-1}$, and $\Gamma=980\text{ cm}^{-1}$ with different values of the cutoff wavelength.

state at low temperature is given by Eq. (3), and with increasing temperature the excited Cr^{3+} sites with energy $\epsilon_- < \epsilon_{\text{cut}}$, where ϵ_{cut} is strongly dependent on temperature T , relax nonradiatively to the ground state. Then, the line-shape function of emission spectrum is

$$I_{\text{em}}(E) = \frac{I_{\text{em}}^0}{\sqrt{2\pi}\Gamma_{\text{em}}} \int_{\epsilon_{\text{cut}}}^{\infty} \exp\left[-\frac{(E' - \epsilon_-)^2}{2\gamma'^2}\right] \times \exp\left[-\frac{(E - E')^2}{2\Gamma^2}\right] dE' \quad (27)$$

The solid curves in Fig. 4(b) were calculated using Eq. (27) with $\epsilon_- = 12050 \text{ cm}^{-1}$, $\gamma' = 230 \text{ cm}^{-1}$, and $\Gamma = 980 \text{ cm}^{-1}$ for different values of ϵ_{cut} . The curves with $\epsilon_{\text{cut}} = 11890, 12020, 12120, \text{ and } 12220 \text{ cm}^{-1}$ (841, 832, 825, and 818 nm) correspond to spectra observed at temperature $T = 80, 170, 260, \text{ and } 300 \text{ K}$. Figure 5 shows the relation between the total intensity and the peak energy of the emission spectra. The observed total intensities are estimated to be twice the area of the spectra from the short-wavelength tail to the peak. The solid curve in Fig. 5 calculated using Eq. (27) fits the observed data quite well.

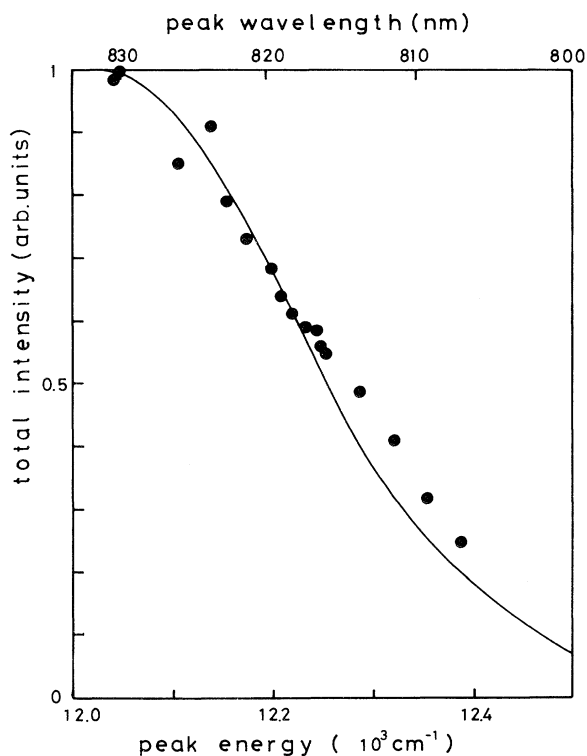


FIG. 5. The relation between the peak energy and the total intensity of the emission spectra of Cr^{3+} :silicate glass excited at 488 nm. The solid curve is estimated from the line shapes calculated using Eq. (27) with the parameter of cutoff wavelength. The observed total intensities are normalized by that at $T = 13 \text{ K}$.

B. Lifetime of Cr^{3+} site with disorder

The luminescence decay time of Cr^{3+} ions in a disordered host at low temperature ($T < 20 \text{ K}$), τ_i , is put equal to τ_1^i in Eq. (15), being determined by mixing coefficients α_i and β_i which are both functions of $\Delta_i = E_i - (S - \frac{1}{2})\hbar\omega - E_i(^2E)$. Figure 6(a) shows the disorder/distribution of Cr^{3+} ion sites as a function of Δ_i where Δ_i and Δ_{max} replace $10Dq = E_i$ and $(10Dq)_0$ in Eq. (3) with an assumption that $S\hbar\omega$ and $E_i(^2E)$ at Cr^{3+} disordered sites are constant. Three distribution functions in Fig. 6(a) are Gaussians having the width of $\gamma' = 150 \text{ cm}^{-1}$ and peaks at $\Delta_{\text{max}} = -100, 0, \text{ and } 100 \text{ cm}^{-1}$. Figure 6(b) shows the distribution as a function of the lifetime τ_1^i using Eqs. (12)–(15) and parameters $\tau_E^i = 6 \text{ ms}$, $\tau_T^i = 60 \mu\text{s}$, $2\delta = 70 \text{ cm}^{-1}$, $\gamma' = 150 \text{ cm}^{-1}$, and $\Delta_{\text{max}} = -100, 0, 100 \text{ cm}^{-1}$.^{7,8} Changing Δ_{max} from negative to positive values shifts the maximum probability to longer lifetimes.

Figure 7 shows that decay curves of the Cr^{3+} luminescence measured at 13 K with different excitation wavelengths: (a) 488, (b) 622, and (c) 579 nm, are nonexponential. Excitation at 488 nm produces only the ${}^4T_2 \rightarrow {}^4A_2$ broadband. The observed decay curves of the broadband at 828 nm denoted by B in Fig. 3 is fitted to the curves calculated using Eqs. (18)–(23) with the parameters $\Delta_{\text{max}} = -130 \text{ cm}^{-1}$, $\gamma' = 150 \text{ cm}^{-1}$, $2\delta = 70 \text{ cm}^{-1}$, $\tau_E^i = 6 \text{ ms}$, and $\tau_{\text{nr}}^i = 60 \mu\text{s}$ in the absence of nonradiative decay term, $W_{\text{nr}}^i(T)$, in Eq. (19). In contrast, the emission spectra excited by laser radiation at 622 and 579 nm consist of the weak R line and the intense broadband in Fig. 3.

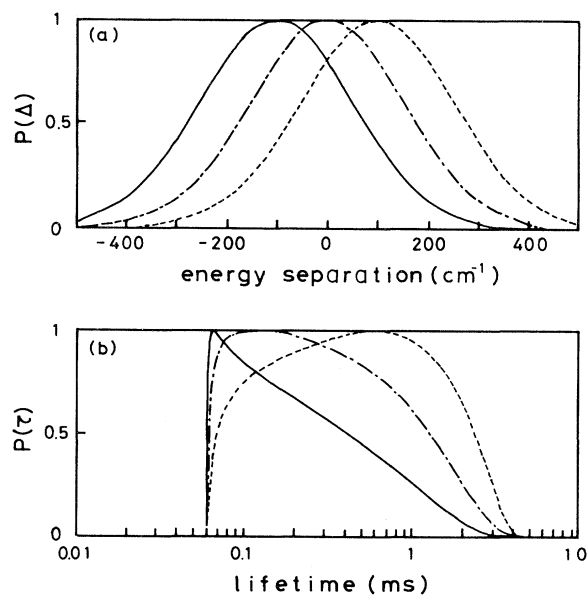


FIG. 6. (a) Disorder distribution as a function of energy separation, $\Delta = E({}^4T_2) - E(^2E) = [10Dq - (S - \frac{1}{2})\hbar\omega] - E(^2E)$. (b) Disorder distribution as a function of the lifetime, τ_1 , in Eq. (15) estimated from the energy separation Δ .

The decay curves of R line at 685 nm denoted by A in Fig. 3 and the broadband at 815 nm denoted by B excited at 622 nm are shown in Fig. 7(b). The decay rate of the R line is about 1 order of magnitude smaller than that of the broadband. The solid curves for the R line and the broadband are calculated using Eqs. (22) and (23), respectively, with the same parameters, $\Delta_{\text{max}} = -110 \text{ cm}^{-1}$, $\gamma' = 150 \text{ cm}^{-1}$, $2\delta = 70 \text{ cm}^{-1}$, $\tau_E^i = 6 \text{ ms}$, and $\tau_T^i = 60 \mu\text{s}$ in the absence of the nonradiative decay term in Eq. (19). In the same way, the decay curves of the R line at 685 nm and the broadband at 805 nm excited at 579 nm, Fig. 7(c), are calculated with the parameters, $\Delta_{\text{max}} = -80 \text{ cm}^{-1}$, $\gamma' = 150 \text{ cm}^{-1}$, $2\delta = 65 \text{ cm}^{-1}$, $\tau_E^i = 6 \text{ ms}$, and $\tau_T^i = 60 \mu\text{s}$. Figure 7(d) shows the decay curves of the emission band with the 488-nm excitation at different temperatures (13, 140, and 250 K). With increasing temperature, the fast

decay components were enhanced. The analysis of the decay curves at high temperature is more complicated than at low temperature, because the decay contains nonradiative term in Eq. (19).

The decay of the Cr^{3+} luminescence at temperature T consists of nonexponential components as shown in Fig. 7. The temperature dependence of the dominant components for the lifetimes of the Cr^{3+} luminescence with different excitations (488, 579, and 622 nm) is shown in Fig. 8. The lifetime of the luminescence excited at 488 nm is short compared to those at 579 and 622 nm. The laser radiation with the 488-nm wavelength located at the longer-wavelength tail of the 4T_1 adsorption broadband excites the Cr^{3+} sites with weaker crystal field. The peak energy of the emission band from the Cr^{3+} sites with the weaker crystal field is shifted to longer wavelength and

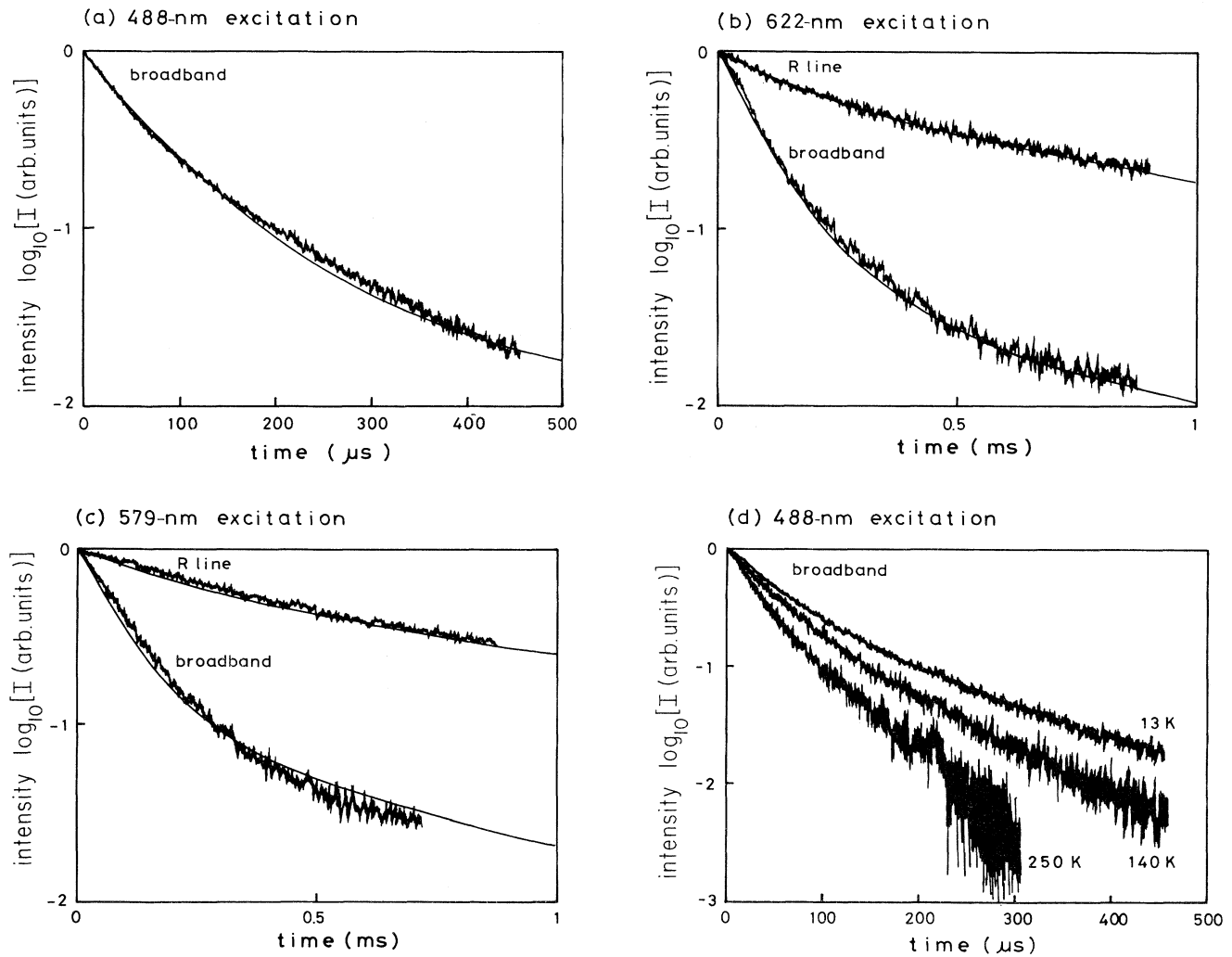


FIG. 7. The decay curves of the Cr^{3+} luminescence in silicate glass at 13 K. (a) 488-, (b) 622-, and (c) 579-nm excitations. Solid curves are calculated using Eqs. (22) and (23) with parameters $\gamma' = 150 \text{ cm}^{-1}$, $2\delta = 70 \text{ cm}^{-1}$, $\tau_E^i = 6 \text{ ms}$, $\tau_T^i = 60 \mu\text{s}$, and $\Delta_{\text{max}} =$ (a) -130 , (b) -110 , (c) -80 cm^{-1} in the absence of the nonradiative decay term in Eq. (19). (d) The decay curves of the broadband excited at 488 nm at different temperatures. The initial intensities of the broadband and the R line are normalized at $t = 0$.

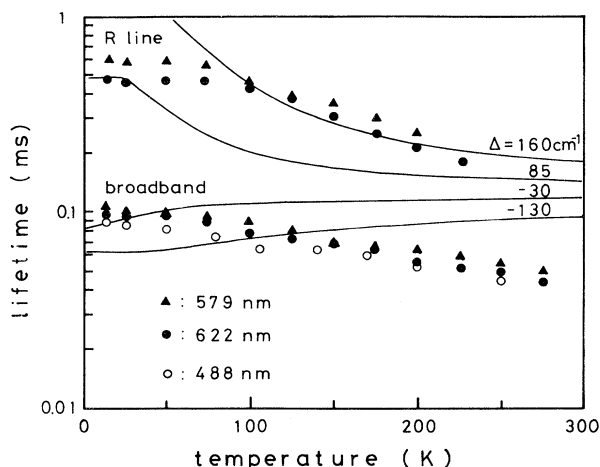


FIG. 8. Temperature dependence of the dominant components of the lifetime for the R line and broadband of Cr^{3+} :silicate glass excited at 579, 622, and 488 nm. Solid curves of the luminescence from a Cr^{3+} site with different energy separations Δ of 160, 85, -30 , and -130 cm^{-1} are calculated using Eq. (19), $2\delta=70 \text{ cm}^{-1}$, $\tau_E^i=6 \text{ ms}$, and $\tau_T^i=60 \mu\text{s}$ in the absence of disorder effect and nonradiative decay term.

their lifetimes become shorter as shown in Fig. 6(b).

The temperature dependence of the lifetime from the disordered Cr^{3+} sites in the silicate glass are very complicated because both disorder effects and nonradiative decay processes are included. First, we consider the temperature dependence of the lifetime from a single Cr^{3+} -ion site in the absence of the nonradiative decay. The solid curves in Fig. 8 are calculated using Eq. (19), $2\delta=70 \text{ cm}^{-1}$, $\tau_E^i=6 \text{ ms}$, and $\tau_T^i=60 \mu\text{s}$ with the variable parameter, energy separation Δ of 4T_2 and 2E excited states in the absence of nonradiative decay rate $W_{nr}^i(T)$. The calculated lifetime of the broadband gradually increases with increasing temperature, whereas the observed lifetime gradually decreases. This discrepancy in the temperature range 100–250 K may be due to lattice expansion which enhances energy separation ($|\Delta|$), giving rise to shortening of the lifetime. The lifetime at temperatures above 250 K is less than $60 \mu\text{s}$ being equal to τ_T for the pure 4T_2 vibronic state. The lifetimes of the R line also decrease rapidly above 250 K. These results suggest that the luminescence decay time from the most stable Cr^{3+} -ion sites in the glass begins to decrease by nonradiative decay above 250 K.

Next, consider the luminescence decay in the presence of the nonradiative transitions from the 4T_2 excited state to the 4A_2 ground state. Figure 9 compares the temperature dependence of the lifetimes of the broadbands excited at 488 nm in the silicate glass with that for $\text{Gd}_3\text{Sc}_2\text{Ga}_3\text{O}_{12}$ (GSGG) crystal reproduced from Aramagan and Di Bartolo.¹⁷ The lifetime of Cr^{3+} :GSGG begins to decrease above 400 K because of the nonradiative decay. The total intensity measured at 550 K is reduced to half that at 77 K. Furthermore, the peak of the emis-

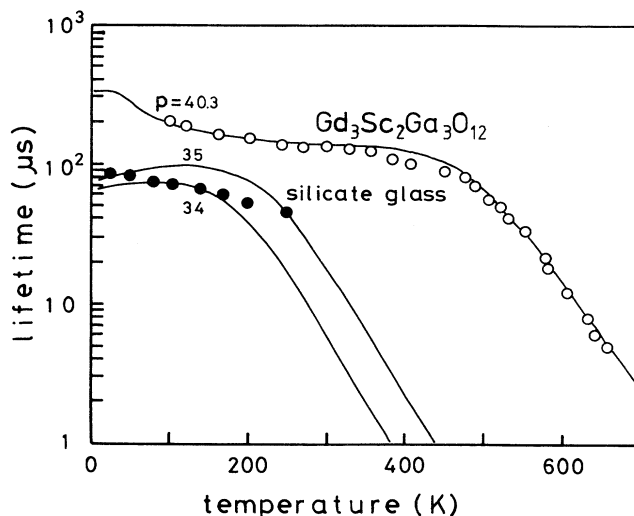


FIG. 9. Temperature dependence of the lifetime of the broadbands of Cr^{3+} in silicate glass and in $\text{Gd}_3\text{Sc}_2\text{Ga}_3\text{O}_{12}$ (GSGG) single crystal. The solid curves are calculated using Eqs. (19) and (25)–(27) with $S=8$, $\hbar\omega=350 \text{ cm}^{-1}$, $\Delta=60 \text{ cm}^{-1}$, $2\delta=70 \text{ cm}^{-1}$, $\tau_E=6 \text{ ms}$, $\tau_T=60 \mu\text{s}$, and $p=40.3$ for Cr^{3+} :GSGG and with $S=8$, $\hbar\omega=350 \text{ cm}^{-1}$, $\Delta=-30 \text{ cm}^{-1}$, $2\delta=70 \text{ cm}^{-1}$, $\tau_E^i=6 \text{ ms}$, $\tau_T^i=60 \mu\text{s}$, and $p=34,35$ for Cr^{3+} :silicate glass.

sion broadband of Cr^{3+} :GSGG, at low temperature, at 740 nm implies a relaxation energy of $S\hbar\omega \sim 1000 \text{ cm}^{-2}$; the spectrum fits a Pekar band shape. With increasing temperature, the wavelength at the peak of the broadband shifts to longer wavelength because of the lattice expansion, this effect being more efficient above 200 K.^{9,17} The peak shift is from 740 nm at 10 K to 840 nm at 577 K. In addition, the emission band shape changes from a Pekar to a Gaussian because of an enhanced Huang-Rhys parameter S . Increasing temperature also changes the crystal field of Cr^{3+} in GSGG from intermediate field ($\Delta \sim 0$) to weak field ($\Delta < 0$).⁵ The solid curve in Fig. 9 is calculated for a single Cr^{3+} site in GSGG using Eqs. (19) and (24)–(26) including terms due to nonradiative decay with $S=8$, $\hbar\omega=350 \text{ cm}^{-1}$ ($S\hbar\omega=2800 \text{ cm}^{-1}$), $\Delta=60 \text{ cm}^{-1}$, $2\delta=70 \text{ cm}^{-1}$, $\tau_E^i=6 \text{ ms}$, $\tau_T^i=60 \mu\text{s}$, and $p=40.3$ ($p\hbar\omega=14100 \text{ cm}^{-1}$). The small difference between the calculated curve and the experimental data in the temperature range 250–450 K is due to the lattice expansion. This effect was discussed in detail by Yamaga *et al.*⁷ In contrast, the emission spectra of the Cr^{3+} :silicate glass at low temperature is very similar to the high-temperature behavior ($T > 500 \text{ K}$) of Cr^{3+} :GSGG, the emission band shape being fitted to a Gaussian due to the weak crystal field ($10Dq \sim 13500 \text{ cm}^{-1}$) with a correspondingly large Stokes shift ($S\hbar\omega \sim 2500 \text{ cm}^{-1}$). The calculated curves for the Cr^{3+} :silicate glass ignore the disorder and use Eqs. (19) and (24)–(26), $S=8$, $\hbar\omega=350 \text{ cm}^{-1}$ ($S\hbar\omega=2800 \text{ cm}^{-1}$), $\Delta=-30 \text{ cm}^{-1}$, $2\delta=70 \text{ cm}^{-1}$, $\tau_E^i=6 \text{ ms}$, and $\tau_T^i=60 \mu\text{s}$ with differential values of p ($p=34,35$). The value of p is a little small compared to that estimated from the observed emission spectrum be-

ing close to 40. To remove the discrepancy between the calculated curve and the observed data requires the inclusion of effects due to disorder and the spectrum of phonons assisting the nonradiative decay process.

The difference in behavior between the silicate glass and the GSGG single crystal is the value of p . Since p , given in Eq. (26), includes the term of the crystal field splitting, $10Dq$, the values for the silicate glass spread through the effect of disorder and are estimated to be in the range of 33–38, rather small compared with that ($p=40.3$) at high temperatures in Cr³⁺:GSGG. The result indicates that the Cr³⁺ ion sites in silicate glass with weaker crystal field relax nonradiatively to the ⁴A₂ ground state at lower temperature.

V. CONCLUSIONS

The Cr³⁺ ions in the silicate glass occupy octahedrally coordinated sites in the damaged SiO₂ network. Site-to-site disorder is apparent in broadened absorption and

emission spectra and the multiexponential luminescence decay patterns. The width of the disorder distribution and the intrinsic width of emission spectrum are estimated to be 150–270 and 965–980 cm⁻¹, respectively, from the above experimental data, the assumption being that both are represented by Gaussians. The large Stokes shift and the weak crystal field at Cr³⁺ sites in the silicate glass compared with those in the GSGG single crystal enhance the nonradiative decay rate from the ⁴T₂ excited state to the ⁴A₂ ground state above 150 K and the emission intensity of Cr³⁺ sites with weaker crystal field is quenched. In consequence, the total intensity of the emission broadband at 300 K is reduced to 25% of the total intensity at 13 K.

ACKNOWLEDGMENT

This work is supported by SERC/MOD Grant No. GR/E 79851.

*Permanent address: Department of Physics, Faculty of General Education, Gifu University, Gifu 501-11, Japan.

¹S. Sugano, Y. Tanabe, and H. Kamimura, *Multiplets of Transition Metal Ions in Crystals* (Academic, New York, 1970).

²B. Henderson and G. F. Imbusch, *Optical Spectroscopy of Inorganic Solids* (Oxford University Press, Oxford, 1989), Chap. 6.

³B. Struve and G. Huber, *Appl. Phys.* **B36**, 195 (1985).

⁴J. P. Hehir, M. O. Henry, J. P. Larkin, and G. F. Imbusch, *J. Phys. C* **7**, 2241 (1974).

⁵B. Henderson, K. P. O'Donnell, M. Yamaga, A. Marshall, and B. Cockayne, *J. Phys. C* **21**, 6187 (1988).

⁶M. Yamaga, B. Henderson, and K. P. O'Donnell, *J. Phys. Condens. Matter* **1**, 9175 (1989).

⁷M. Yamaga, B. Henderson, K. P. O'Donnell, C. Trager-Cowan, and A. Marshall, *Appl. Phys. B* **50**, 425 (1990).

⁸M. Yamaga, B. Henderson, K. P. O'Donnell, and Y. Gao, *Appl. Phys. B* **51**, 132 (1990).

⁹C. J. Donnelly, S. M. Healy, T. J. Glynn, G. F. Imbusch, and

G. P. Morgan, *J. Lumin.* **42**, 119 (1988).

¹⁰F. Rasheed, K. P. O'Donnell, B. Henderson, and D. B. Hollis, *J. Phys. Condens. Matter* **3**, 1915 (1991).

¹¹F. Rasheed, K. P. O'Donnell, B. Henderson, and D. B. Hollis, *J. Phys. Condens. Matter* **3**, 3825 (1991).

¹²R. Englman, *Non-radiative Decay of Ions and Molecules in Solids* (North-Holland, Amsterdam, 1979).

¹³W. H. Fonger and C. W. Struck, *J. Chem. Phys.* **69**, 4171 (1978).

¹⁴T. Bates and R. W. Douglas, *J. Soc. Glass Technol.* **43**, 289 (1959).

¹⁵R. E. Tischer, *J. Chem. Phys.* **48**, 4291 (1968).

¹⁶J. L. Andrews, A. Lempicki, and B. C. McCollum, *J. Chem. Phys.* **74**, 5526 (1981).

¹⁷G. Armagan and B. Di Bartolo, in *Tunable Solid-State Laser II* edited by A. B. Budgor, L. Esterowitz, and L. G. DeShazer (Springer-Verlag, Berlin, 1986), pp. 35–43.